

Automated model for identification on mastoid of temporal bone image

Syafri Arlis¹, Sarjon Defit², Sumijan³

¹Department of Informatics Technology, Faculty of Computer Science, University Putra Indonesia YPTK, Padang, Indonesia

²Doctoral Program in Information Technology, University Putra Indonesia YPTK, Padang, Indonesia

³Information Technology, Faculty of Computer Science, University Putra Indonesia YPTK, Padang, Indonesia

Article Info

Article history:

Received Oct 17, 2022

Revised Mar 15, 2023

Accepted Mar 24, 2023

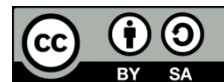
Keywords:

Automated identification
Computed tomography-scan
Extended adaptive threshold
Mastoid air cell system
Segmentation
Temporal bone

ABSTRACT

Mastoiditis occurs due to inflammation that can affect the structure of the mastoid bone. The mastoid bone consists of the mastoid air cell system (MACS) which protects the ear structures and regulates air pressure in the ear and has different sizes and characteristics, making it very difficult to identify precisely. This study aims to identify and find the right MACS size by developing an automatic identification model and obtaining the optimal threshold value in the segmentation process using the extended adaptive threshold (eAT) method. The research dataset uses computed tomography (CT)-scan images of 308 slices of 12 patients indicated for mastoiditis. The results of this study provide identification that has the right MACS accuracy and size. Overall, the optimal segmentation process obtained the smallest threshold value of 57 and the largest threshold value of 63, the smallest MACS size is 4.025 cm² and the largest is 8.816 cm² with an accuracy rate of 93.4%. The smaller MACS size indicates inflammation in the mastoid area and these patients require more intensive treatment.

This is an open access article under the [CC BY-SA](https://creativecommons.org/licenses/by-sa/4.0/) license.



Corresponding Author:

Syafri Arlis

Department of Informatics Technology, Faculty of Computer Science, Universitas Putra Indonesia YPTK

Padang, West Sumatra, Indonesia

Email: syafri_arlis@upiyptk.ac.id

1. INTRODUCTION

The ear is a sensory organ that is responsible for hearing in the human body [1]. Healthy hearing will increase productivity in life. Most people in developing countries live with hearing loss. More than 5% of the number of hearing sufferers of the world's population, where this disorder affects almost 34 million children. In 2050, nearly 2.5 billion people worldwide or 1 in 4 people live with some degree of hearing loss. At least 700 million people need hearing rehabilitation care and services [2].

Indonesia is one of the four countries in Southeast Asia with the highest prevalence rate of hearing loss, namely 4.6% along with India (6.3%), Myanmar (8.4%) and Sri Lanka (8.8%). Nationally, 2.6% of people experience hearing loss with a deafness prevalence rate of 0.09%. Hearing loss is now often overlooked because it is considered not to cause death. This opinion is very wrong, because if left unchecked continuously can lead to inflammation such as otitis media and bone erosion and damage to surrounding organ structures which eventually lead to complications and can even lead to stroke due to complications to the brain [3], [4].

Mastoiditis is a complication of chronic suppurative otitis media due to bacterial infection that occurs in the mastoid bone [5], [6]. This infection spreads from the ear to the mastoid air cell system (MACS) which can damage the bone structure of the ear, making it difficult to diagnose and decide on surgery [7], [8]. The mastoid bone has many cavities and must have fluent airflow to function properly.

Today's technology has had a significant influence on every aspect of human life [9]. In recent times, technology has penetrated all fields, such as health, economics, society, culture, and others [10]. Furthermore, technology in the medical field has certainly provided input and improvements to support the performance of the health world [11]. The role of technology in the health sector is also able to provide positive trends in assisting medical personnel in carrying out the diagnosis process [12].

The form of application of this technology can be seen from the use of computed tomography scan (CT-scan) technology to support the diagnosis process [13]. The diagnostic process is carried out to facilitate the process of identifying a disease that is difficult to detect [14]. One of the diseases that can be detected with this CT-scan is the MACS in the temporal bone [15].

CT-scan is an imaging examination performed on patients suffering from mastoiditis to detect abnormalities in the temporal bone and to describe small features of the inner ear [16], [17]. CT-scan has become an important way to examine the anatomical organs of the human temporal bone in the diagnosis and treatment of ear diseases [18]. This examination has not been able to fully assist doctors in determining the diagnosis, because it is still determined from the patient's clinical history and evaluation of doctor's care [19], and it is difficult to determine the segmentation of the size of the inner ear on the temporal bone structure [20].

The application of image processing technology is the right solution to identify the presence and measure the MACS area on the mastoid bone. Several studies in processing CT-scan images of mastoid bone from patients with mastoiditis, such as analyzing the presence and extracting MACS using surface skeleton and curve skeleton techniques and extracting geometric information from MACS objects [21]. Furthermore, the segmentation process is carried out automatically using the morphological image enhancement and convolutional neural network (CNN) method to describe the region of interest (ROI) structure of the Temporal bone micro-object from the CT-scan image. This study resulted in a good accuracy of detection and identification of temporal bone structure [22]. Further research uses the segmentation method by manually determining the threshold value in calculating the MACS surface area and volume based on the value of hounsfield unit (HU) [23]. The same study evaluated the value of HU in differentiating right and left-sided MACS and associating with patient age [24].

Anatomical segmentation of ear structures using the CNN method combined with 2D Segmentation methods (U-Net, ResU-Net, SEU-Net), 3D volume mask and region extraction. This study resulted in a fairly good segmentation of several objects to be analyzed [25]. Furthermore, semi-automatic CT-scan reconstruction in measuring the volume of inner ear structures using global thresholding and feature region segmentation methods. The results of this study can reconstruct 3D volume, but it is difficult to determine the segmentation of the size of the inner ear on the temporal bone structure because of the size, many characteristics of the same object and overlapping and the position of the structure on the temporal bone is different at the time of shooting [26].

This study proposes an update in the process of segmentation and automatic identification of MACS objects on the axial CT-scan of the temporal bone. The research results can identify and determine the size of the MACS surface area very well. Thus, this study can be used as a recommendation model for identifying the severity of MACS for medical parties in the management of further treatment.

2. METHOD

The research dataset used the results of CT-scan mastoid images from the temporal bone of axial slices as many as 308 slices of images of 12 patients suffering from mastoiditis. The image is taken using a CT-scan that uses x-rays as a source that penetrates the organs of the body, then the rays are captured by a detector and reconstructed by a computer into a digital image. The images tested in this study are images of the results of an axial scan of the temporal bone for patients with mastoiditis in the radiology section of the Dr. Central General Hospital. M. Djamil Padang, West Sumatera, Indonesia. The image was taken using a Siemens SOMATOM Perspective CT-scanner and the results can be viewed with the syngo® fastView application and saved as a digital image in the joint photographic group (JPG.) format. The test image used was taken from the axial CT-scan of the temporal bone, as shown in Figure 1. Figure 1(a) shows an overview of the MACS and Figure 1(b) is the result of a CT scan of the temporal bone of a patient with mastoiditis. Then it was applied to the automatic identification model in Figure 2 to identify the presence of MACS.

Figure 1 is the result of an axial CT-scan of the temporal bone. Figure 1(a) is an object of inflammation in the mastoid area and Figure 1(b) shows an overall picture of the results of a CT-scan image of the temporal bone. Based on these results, the CT-scan image still requires further image processing to determine the presence of an amorphous and narrowed MACS. Thus, the identification process in measuring the area of the MACS is needed to ensure the diagnosis results. The process can be presented in the research framework presented in Figure 2.

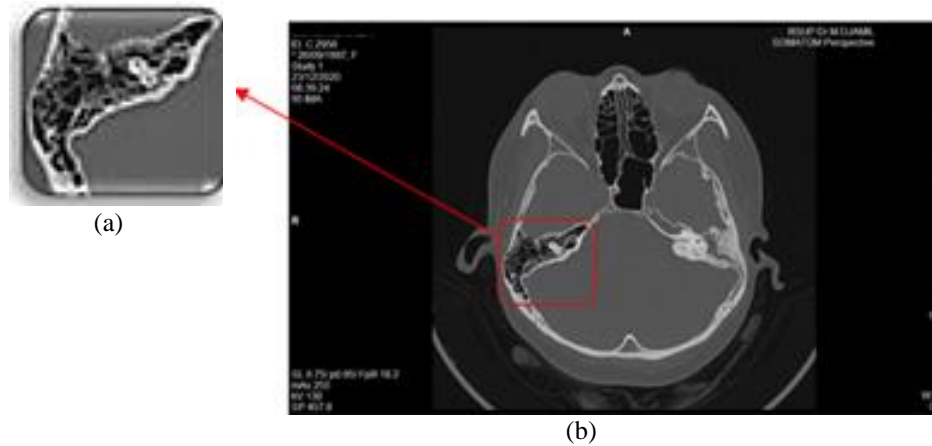


Figure 1. The Axial CT-scan of the temporal bone (a) mastoid air cell system and (b) CT-scan temporal of patients with mastoid

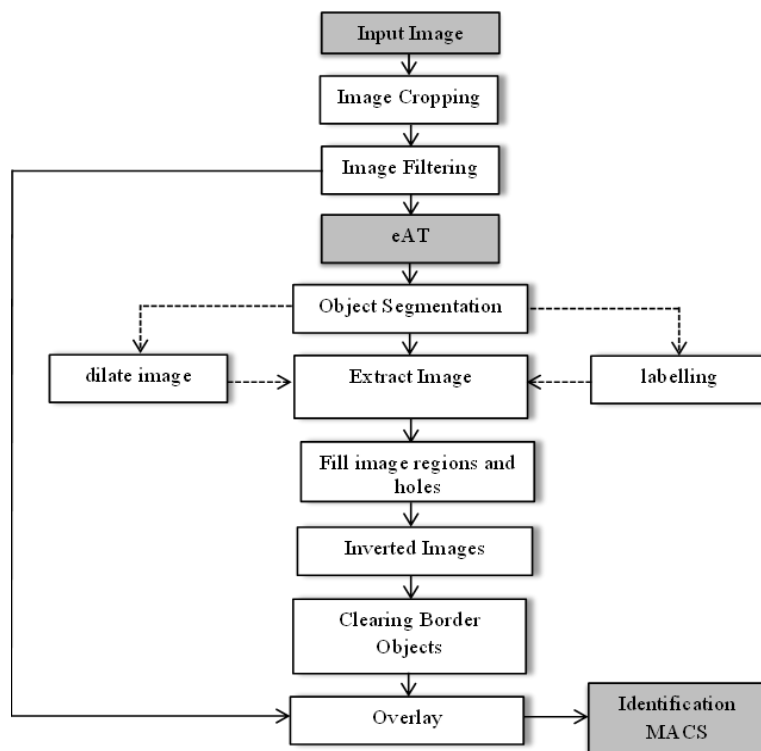


Figure 2. Research framework

Figure 2 describes the research framework presented by image processing in identification. This process was developed to have automatic performance in determining the air cell system on temporal CT-scan images. Several stages of image processing are used to produce precise and accurate output. The stages of the process consist of image cropping, image enhancement, and binary image conversion by calculating the optimal threshold value, morphological operations, and region properties. All these stages will be developed in an algorithmic model in the identification of air cell systems on temporal CT-scan images.

2.1. Image filtering

This stage aims to eliminate small variations between neighboring pixels by adjusting the pixel value to the histogram value level [27], [28], thus clarifying and improving image quality for processing at next stage. The filtering process used in (1).

$$mf(x, y) = median_{(p,q) \in S_{xy}} \{x(p, q)\} \tag{1}$$

Where $mf(x, y)$ is the result of the median filter, $median_{(p,q) \in S_{xy}}$ is the average value of the pixel coordinates of $x(p, q)$. The median filter process results in filtering the position of pixel values which are moved sequentially from the smallest pixel value to the largest pixel value for the overall pixel value in the image. Furthermore, the position of the pixel values that have been sorted is determined by the middle value (median) and used as the value between pixels.

2.2. Extended adaptive threshold (EAT)

The segmentation process aims to separate the object region from the background region so that objects in the image are easy to analyze in recognizing objects and classifying objects [29]. Due to the large number of visual characteristics of the object displayed on the axial CT-scan of the temporal bone, it is necessary to separate the mastoid area from unnecessary CT-scan input images. However, the results of CT-scan images vary depending on the difficulty of the image, the color, the position of the area around the mastoid and the brightness level of the image [30]. Threshold segmentation methods that can be used in the segmentation process are single threshold and multi threshold [31]. In general, the threshold segmentation method used is the Otsu method by taking into account the maximum class variance value [32], [33]. The segmentation approach using the multi-level Otsu method can predict the desired optimal threshold point by calculating the histogram and probability in a homogeneous region based on the gray scale color intensity level to separate objects from the background and convert binary images [34], [35]. The pixel feature value is compared with the segmentation threshold in order to determine which part of the image to group [36], [37]. Calculation of the mathematical formula for the Otsu threshold by calculating the intensity value of the gray level is presented in (2).

$$p_1 = \sum_{i=T}^{K-1} p_i = 1 - p_0 \tag{2}$$

In (2) is a process for calculating the overall pixel intensity value with a gray level of 'K' as [0, K-1] at each p_i pixel intensity level. The results of these calculations can maximize the variance between classes of each pixel intensity value with a grayscale. To calculate the probability value for each grayscale pixel intensity value is presented in (3).

$$p_i = \frac{n_i}{N} (p_i > 0) \tag{3}$$

In (3) is a calculation to determine the distribution of gray level intensity in an image. N is the sum of all pixel intensities in the image and n_i is the number of pixel intensities i . Calculating the optimal threshold value for the input image proposed in this study to separate objects from the background is presented in (4).

$$eAT = \frac{\sum_{i:n} k \cdot h_i}{\sum_{i:n} p_i} \tag{4}$$

In (4) is the calculation of the optimal threshold value with the eAT method for each test image, where $\sum_{i:n} k \cdot h_i$ calculate the total pixels overall against the intensity of the pixel value with the degree of gray from the normalized histogram to i , then divided by the average number of intensity values of the gray level of a grayscale image expressed by $\sum_{i:n} p_i$. The value ranges from 1 to n, with a maximum value of n=255. Figure 3 illustrates the process of image threshold values.



Figure 3. Extended adaptive threshold process

Figure 3 is the conversion result of the gray image to a binary image using the optimal threshold value with the eAT algorithm. Image pixel values that exceed or are less than the threshold value is grouped into certain areas. Furthermore, the results of this binary image are applied to the identification model for the next process stage.

2.3. Object extraction method

This stage aims to extract information from the object to be analyzed and differentiated from several other objects that have unique intensity and characteristics values [38], [39]. In carrying out the object extraction process, an image that has been generated from the segmentation and morphology process is needed with the aim of obtaining characteristics that can distinguish an object from other objects in the image [40]. To distinguish the features of the object to be analyzed, the separation is carried out by calculating the pixel statistics on the image object and determining the input value or parameter [41]. The parameters used in object extraction are shown in the (5).

$$metric_i = 4\pi \left[\frac{a_i}{p_i^2} \right] \quad (5)$$

Ratio of the metrics can be calculated from the area and circumference of the image with a_i maximum intensity value of 1 only for circles and less than 1 for other shapes. The results of calculating the value ratio are used to extract the desired object by trading the binary value of each object in the image. After the object separation process is carried out in the image, the steps are continued to remove small parts of the object that are not processed. The results of the process are presented in a closing morphological reconstruction model involving several previously processed images and a steel.

2.4. Morphological operations

After getting the image results from the image segmentation and extraction process, the next step is to perform morphological operations based on the morphological features of the image [42], [43]. Morphology is an image processing process that focuses on the shape of objects [44]. Filling region is one of the morphological algorithms in image processing with the aim of selecting an area with a certain color [45]. Figure 4 shows an illustration of the filling region method process, where Figure 4(a) is the input image to be analyzed, Figure 4(b) shows the results of the one region fill process and Figure 4(c) is the result of the all region fill process.

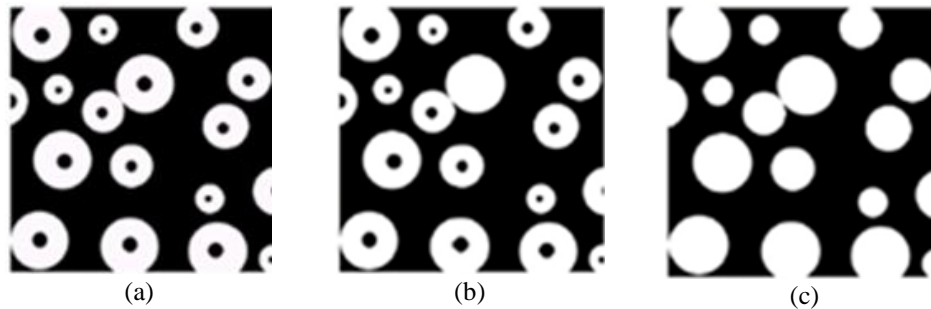


Figure 4. Illustration of the filling region method process, (a) original image, (b) one region fill, and (c) all region fill

Figure 4 is an illustration of the results of the morphological operation process in segmentation. In more detail, Figure 4(a) is the original image, Figure 4(b) is the result of one region filling image, and Figure 4(c) is the result of the morphological operation of the region-filling. The results of the process described in the morphological operation present an overview of obtaining the surface area of the object.

2.5. Inverted image

This stage is a simple operation performed in image processing. This process reverses the value of the image with a positive value to be negative and vice versa [46]. This process clarifies the intensity of the object needed to be analyzed in the next stage. The inverted image process equation is presented in the (6) [47].

$$I_{(x,y)} = K + 1 + L_{(x,y)} \quad (6)$$

Where $I_{(x,y)}$ is the result of the process of reversing the intensity value, K is the minimum value and $L_{(x,y)}$ is the initial intensity value. This process is to get a negative image, so to find a negative value subtract the maximum value. Figure 5 shows an illustration of the inverted image process, where Figure 5(a) is the result of the input image to be analyzed and Figure 5(b) shows the result of the image negation process.

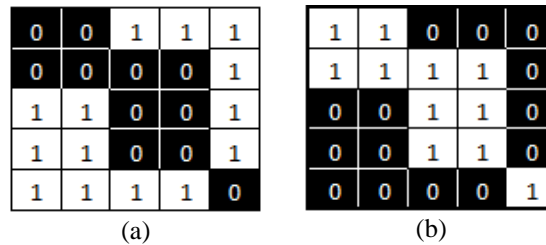


Figure 5. The process of inverted images (a) original image and (b) inverted process results

Figure 5 shows the black pixel value (0) which will be replaced with the white pixel value (1). This process stage reverses the pixel value in the initial image from a positive value to a negative value. The results of this process can obtain accurate results when eliminating noise and clarifying the image.

2.6. Clearing border and overlay

This stage aims to clean objects with some noise around the image area, where non-region of interest (non-ROI) objects that are connected to the image boundary need to be removed [48]. Furthermore, this result is carried out with an image overlay with the aim of focusing the object on a particular image by covering the main object and displaying object identification (OII) which is the main focus [49]. By using an image overlay on medical images, it is possible to know the exact anatomy and visualize the anatomy of the temporal bone, especially MACS, thus potentially increasing the surgeon's analysis in performing a series of more complex examination procedures.

3. RESULTS AND DISCUSSION

In this study using test data with 1 patient, where the image of the patient being tested consists of 193 slices of images of mastoiditis patients. From the many slices of the image, 7 slices of images of patients with mastoiditis who still have MACS are taken from both the right and left sides, namely the slices of image 95 to slices of image 101. The input image is converted from the syngo® fastView application with a size of 1105 x 649 pixels with the format JPG. Some of the information contained in the image has been omitted in order to maintain the code of ethics with the image cutting process, The description of the input image can be presented in Figure 6.



Figure 6. Input image

Figure 6 is the input image used in the identification process. The image uses the results of a temporal CT-scan image. The discussion process begins with performing image preprocessing by adopting cropping and filtering operations with the aim of improving image quality. The image enhancement process can present output which can be seen in Figure 7, where Figure 7(a) is the result of image cropping which will be analyzed by a filtering process to improve image quality as shown in Figure 7(b).

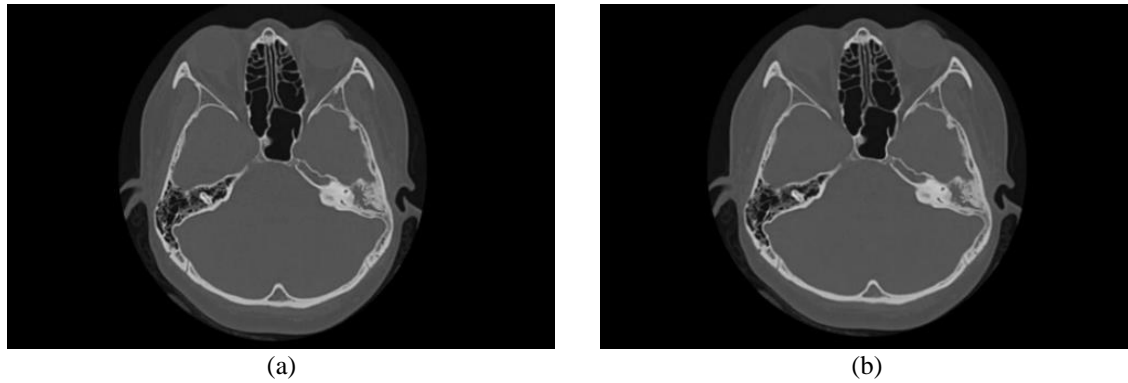


Figure 7. Image enhancement process (a) cropped image and (b) image filtering results

Figure 7 is the image processing stage of the input image which aims to produce better image quality than the previous image. Figure 7(a) is the result of the image cropping process which is capable of displaying predetermined objects. Furthermore, a filtering process is carried out to improve the quality of the image which will be processed at a later stage as shown in Figure 7(b). The filtering results resulted in the changes presented in Table 1.

Table 1. Intensity value

Image cropping									Image filtering								
97	110	119	119	111	100	93	91	97	97	110	119	114	111	100	95	95	98
110	121	124	119	107	96	90	91	99	110	121	119	119	107	96	93	93	99
124	128	122	112	101	94	91	94	102	124	124	121	112	100	93	91	93	101
135	130	114	100	93	91	91	93	101	128	127	114	101	93	91	91	93	101
143	127	103	88	85	87	89	91	96	135	127	103	93	87	87	89	91	96
146	122	94	80	81	85	87	88	91	143	122	94	85	85	85	87	88	91
143	115	89	78	80	85	87	88	87	141	115	89	81	81	85	87	88	88
134	107	86	79	82	87	89	89	87	141	107	86	82	82	87	89	88	88
120	97	84	82	86	89	90	90	88	117	97	85	84	86	89	89	89	88
105	88	82	85	89	90	89	90	89	104	88	84	85	89	89	90	89	88
93	81	81	86	90	90	89	89	88	93	82	82	85	89	89	89	89	88
85	79	80	85	89	90	89	89	87	85	81	81	85	89	89	89	89	87
83	79	80	84	87	89	90	88	85	85	81	81	84	87	89	89	88	85
88	82	81	83	86	89	89	88	85	88	82	82	83	86	89	89	88	85
100	87	81	82	86	88	89	86	83	96	87	82	82	86	88	88	86	83

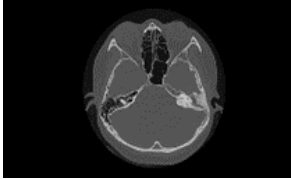

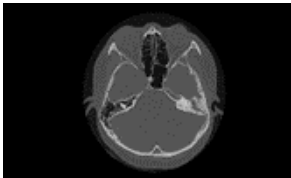

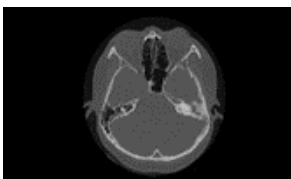








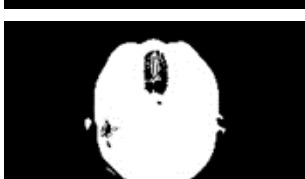
The results of this filtering process are then converted to binary images, where at this stage the conversion process performs an automatic threshold value calculation for each input image with the development of the thresholding method. The goal is to get an optimal threshold value in separating the object to be analyzed as the foreground from the background. The value of each pixel is changed to 0 (zero) if it has the same small value as the threshold value and vice versa if the large pixel value of the threshold is changed to 1 (one). The results of this process for each patient are presented in Table 2.

The results of the development of the eAT method for the binary image conversion process are as shown in Table 2, where for each input image a different optimal threshold value is obtained automatically. Furthermore, the results of this binary image are applied to the development of the designed model. The next

stage is an automatic identification process by performing object extraction and morphological reconstruction to remove unnecessary objects and highlight MACS image object identification (OII).

The results of OII MACS are image negation process, each pixel value of the image with a value of 0 is changed to 1 and vice versa each pixel value of 1 is changed to 0. Image negation results distinguish the objects identified in the image so that the object image is cleaned from some of the noise in the object image. with similar intensity values (neighboring images), where non-ROI objects that are connected to the image boundary have improved quality and separated OII MACS.


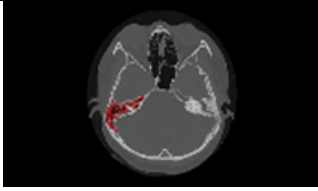

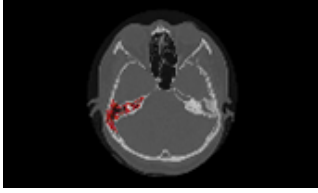



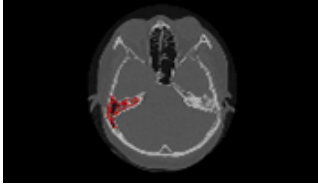
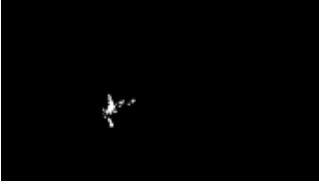

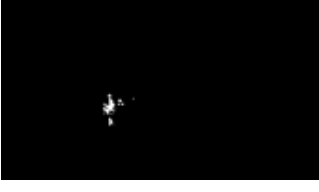

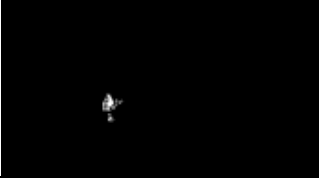
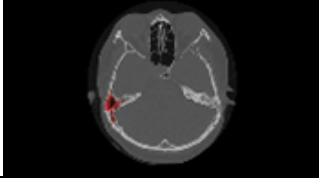
Table 2. Binary image results of eAT

	Image results of filtering process	Binary image results of eAT	Value of eAT
Slice 1			63
Slice 2			61
Slice 3			61
Slice 4			59
Slice 5			58
Slice 6			58
Slice 7			57

The final stage of the development of this model is the MACS size calculation process from OII MACS, the calculation is carried out by calculating the white pixel intensity value (value 1), each pixel is

converted to mm worth 0.29 (1 pixel=0.29 mm). For each identified pixel, the pixel value is changed to red. The results of extraction, identification and calculation of MACS size are presented in Table 3.

Table 3. Extraction results, identification, and area MACS

	MACS extraction results	MACS identification	Pixel area	Area (cm ²)
Slice 1			3040	8.816
Slice 2			2827	8.198
Slice 3			3040	8.816
Slice 4			2399	6.957
Slice 5			2229	6.464
Slice 6			1681	4.875
Slice 7			1388	4.025

The results in Table 3 show that MACS OII was identified with very good accuracy so that the MACS size can be calculated precisely. The calculation used to determine the accuracy is shown in the (7).

$$\text{Accuracy \%} = \frac{\sum OII_{MACS}}{\sum \text{Data Testing}} \times 100\% \quad (7)$$

Where the level of accuracy is the number of MACS objects identified against the number of images tested multiplied by 100%. The smallest MACS size from this study was 4.025 cm² and the largest size was 8.816 cm² with an accuracy rate of 93.4%. Identified MACS area provides information in the form of MACS object area. The smaller MACS size indicates inflammation in the mastoid area and these patients require more intensive treatment.

Based on the previous explanation, the segmentation process with the proposed method of identifying MACS objects automatically provides precise and accurate output. This research is able to present a novelty in the image segmentation process on CT-scan. thus this research can make a positive contribution which is used as an alternative solution in the diagnosis process. Another impact of this research is that it can provide accuracy in decision-making for the process of treating patients with mastoiditis.

4. CONCLUSION

The process of developing a segmentation method for the detection of the MACS provides precise and accurate identification results. The development of the segmentation method is able to maximize the performance of the previous identification process by providing information on the volume of the MACS. Based on the results of the tests carried out, the method development also provides new knowledge with the optimal threshold value automatically on each patient test image slice. Overall, the results provided by this study have a major contribution in determining mastoiditis disease for the medical side in making decisions regarding the follow-up of further treatment.

ACKNOWLEDGEMENTS

Thanks to Mrs. dr. Tuti Handayani, Sp.Rad as a Radiology Doctor at RSUP DR. M. Djamil Padang, West Sumatra as an expert in validating the results of this research based on the license from the Faculty of Computer Science UPI-YPTK Padang No.005/PSTI/UPI-YPTK/IP/XI/2020 and official note from the Head of Research and Development Unit RSUP DR. M. Djamil Padang No. LB.01.02/1.3/S427/2020 regarding the appointment of experts in this research.

REFERENCES




- [1] S. Anandamurugan, M. S. Kumar, E. G. Prashanth, and K. Nithin, "Ear disease detection using R-CNN," in *2022 Fifth International Conference on Computational Intelligence and Communication Technologies (CCICT)*, 2022, pp. 543-549, doi: 10.1109/CCICT56684.2022.00101.
- [2] M. Roccio, P. Senn, and S. Heller, "Novel insights into inner ear development and regeneration for targeted hearing loss therapies," *Hear. Res.*, vol. 397, 2020, doi: <https://doi.org/10.1016/j.heares.2019.107859>.
- [3] N. R. Sayal, S. Boyd, G. Z. White, and M. Farrugia, "Incidental mastoid effusion diagnosed on imaging: Are we doing right by our patients?," *Laryngoscope*, vol. 129, no. 4, pp. 852-857, 2019, doi: 10.1002/lary.27452.
- [4] P. Cassano, G. Ciprandi, and D. Passali, "Acute mastoiditis in children," *Acta Biomedica*, vol. 91, no. 1, pp. 54-59, 2020, doi: 10.23750/abm.v91i1-S.9259.
- [5] S. Jain, P. Singh, D. Methwani, and S. Kalambe, "Role of eustachian dysfunction and primary sclerotic mastoid pneumatization pattern in aetiology of squamous chronic otitis media: a correlative study," *Indian Journal of Otolaryngology and Head and Neck Surgery*, vol. 71, pp. 1190-1196, 2019, doi: 10.1007/s12070-018-1259-x.
- [6] S. L. Purchase, V. I. Bazaliiskii, and A. R. Lieverse, "An innovative method to visualise mastoiditis using a hand-held X-ray system," *International Journal of Paleopathology*, vol. 26, no. May, pp. 22-26, 2019, doi: 10.1016/j.ijpp.2019.05.006.
- [7] M. W. Mather, P. D. Yates, J. Powell, and I. Zammit-Maempel, "Radiology of acute mastoiditis and its complications: A pictorial review and interpretation checklist," *The Journal of Laryngology and Otology*, vol. 133, no. 10, pp. 856-861, 2019, doi: 10.1017/S0022215119001609.
- [8] D. H. Toneva, S. Y. Nikolova, D. K. Zlatareva, V. G. Hadjidekov, and N. E. Lazarov, "Sex estimation by mastoid triangle using 3D models," *Homo*, vol. 70, no. 1, pp. 63-73, 2019, doi: 10.1127/homo/2019/1010.
- [9] S. S. Olimov and D. I. Mamurova, "Information technology in education," *Procedia Computer Science*, vol. 1, pp. 17-22, 2022, doi: 10.1016/j.procs.2010.12.062.
- [10] H. Schiele, A. Bos-Nehles, V. Delke, P. Stegmaier, and R.-J. Torn, "Interpreting the industry 4.0 future: technology, business, society and people," *Journal of Business Strategy*, vol. 43, no. 3, pp. 157-167, 2022, doi: 10.1108/JBS-08-2020-0181.
- [11] A. A. Nishonov and N. F. Nuriddinova, "Introduction of molecular diagnostics and new technologies in modern medical and biological examinations," *Toshkent Tibbiyot Akademiyasi Zamonaviy Klinik Laborator Tashxisi Dolzarb Muammolari*, 2022.
- [12] C. Yu and E. J. Helwig, "The role of AI technology in prediction, diagnosis and treatment of colorectal cancer," *Artificial Intelligence Review*, vol. 55, pp. 323-343, 2022, doi: 10.1007/s10462-021-10034-y.
- [13] D. Andreini *et al.*, "Comprehensive evaluation of left ventricle dysfunction by a new computed tomography scanner: the E-PLURIBUS study," *Cardiovasc. Imaging*, vol. 16, no. 2, pp. 175-188, 2023, doi: 10.1016/j.jcmg.2022.08.005.
- [14] R. B. Seah, W.-K. Mak, K. Bryant, M. Korlaet, A. Dwyer, and G. I. Bain, "Four-dimensional computed tomography scan for dynamic elbow disorders: recommendations for clinical utility," *JSES International*, vol. 6, no. 1, pp. 182-186, 2022, doi: 10.1016/j.jseint.2021.09.013.
- [15] M. Khosravi, Y. J. Moghaddam, M. Esmaceli, A. Keshtkar, J. Jalili, and H. T. Nasrabadi, "Classification of mastoid air cells by CT scan images using deep learning method," *Journal Big Data*, vol. 9, no. 1, pp. 1-14, 2022, doi: 10.1186/s40537-022-00596-1.
- [16] H. Rodrigues *et al.*, "Mastoid, middle ear and inner ear analysis in CT scan-a possible contribution for the identification of remains," *Medicine, Science and the Law*, vol. 60, no. 2, pp. 102-111, 2020, doi: 10.1177/0025802419893424.
- [17] Z. Mughal, A. R. Charlton, and M. Clark, "The prevalence of incidental mastoid opacification and the need for intervention: a meta-analysis," *Laryngoscope*, vol. 132, no. 2, pp. 422-432, 2022, doi: 10.1002/lary.29581.

- [18] S. Manik, Y. Dabholkar, S. Bhalekar, H. Velankar, N. Chordia, and A. Saberwal, "Sensitivity and specificity of high-resolution computed tomography (HRCT) of temporal bone in diagnosing cholesteatoma and its correlation with intraoperative findings," *Indian Journal of Otolaryngology and Head and Neck Surgery*, 2020, doi: 10.1007/s12070-020-01892-z.
- [19] D. J. Lafferty, J. E. Cohn, and B. J. McKinnon, "Incidental mastoid opacification on computed tomography in the pediatric population," *International Journal of Pediatric Otorhinolaryngology*, vol. 128, no. January 2019, 2020, doi: 10.1016/j.ijporl.2019.109688.
- [20] A. Bouchana, J. Kharroubi, and M. Ridal, "Semi-automatic algorithm for 3D volume reconstruction of inner ear structures based on CT-scan images," *In 2018 4th International Conference on Advanced Technologies for Signal and Image Processing (ATSIP)*, pp. 1-6, 2018, doi: 10.1109/ATSIP.2018.8364474.
- [21] O. Cros, M. Gaihede, A. Eklund, and H. Knutsson, "Surface and curve skeleton from a structure tensor analysis applied on mastoid air cells in human temporal bones," *Proc. - Int. Symp. Biomed. Imaging*, vol. i, pp. 270-274, 2017, doi: 10.1109/ISBI.2017.7950517.
- [22] Y. Lv, J. Ke, Y. Xu, Y. Shen, J. Wang, and J. Wang, "Automatic segmentation of temporal bone structures from clinical conventional CT using a CNN approach," *In 2017 IEEE 14th International Symposium on Biomedical Imaging (ISBI 2017)*, vol. 17, no. 2, pp. 1-9, 2021, doi: 10.1002/rcs.2229.
- [23] E. M. Pinto *et al.*, "Efficacy of Hounsfield Units Measured by Lumbar Computer Tomography on Bone Density Assessment: A Systematic Review," *Spine (Phila. Pa. 1976)*, vol. 47, no. 9, pp. 702-710, May 2022, doi: 10.1097/BRS.0000000000004211.
- [24] L. Munhoz, C. H. Iida, R. A. Júnior, R. Abdala, and E. S. Arita, "Mastoid air cell system: Hounsfield density by multislice computed tomography," *Journal of Clinical and Diagnostic Research*, vol. 12, no. 4, pp. TC01-TC03, 2018, doi: 10.7860/JCDR/2018/34463.11366.
- [25] R. Hussain, A. Lalonde, K. B. Girum, C. Guigou, and A. Bozorg Grayeli, "Automatic segmentation of inner ear on CT-scan using auto-context convolutional neural network," *Scientific Reports*, vol. 11, no. 1, pp. 1-10, 2021, doi: 10.1038/s41598-021-83955-x.
- [26] X. Li, Z. Gong, H. Yin, H. Zhang, Z. Wang, and L. Zhuo, "A 3D deep supervised densely network for small organs of human temporal bone segmentation in CT images," *Neural Networks*, vol. 124, pp. 75-85, 2020, doi: 10.1016/j.neunet.2020.01.005.
- [27] M. Viscaino, J. C. Maass, P. H. Delano, M. Torrente, C. Stott, and F. Auat Cheein, "Computer-aided diagnosis of external and middle ear conditions: A machine learning approach," *PLoS One*, vol. 15, no. 3, pp. 1-18, 2020, doi: 10.1371/journal.pone.0229226.
- [28] J. Na'am *et al.*, "Detection of infiltrate on infant chest X-ray," *TELKOMNIKA (Telecommunication Comput. Electron. Control)*, vol. 15, no. 4, pp. 1943-1951, 2017, doi: 10.12928/TELKOMNIKA.v15i4.3163.
- [29] S. Tongbram, B. A. Shimray, and L. S. Singh, "Segmentation of image based on k-means and modified subtractive clustering," *Indonesian Journal of Electrical Engineering and Computer Science (IJECS)*, vol. 22, no. 3, pp. 1396-1403, 2021, doi: 10.11591/ijeecs.v22.i3.pp1396-1403.
- [30] H. Asaturyan, A. Gligorievski, and B. Villarini, "Morphological and multi-level geometrical descriptor analysis in CT and MRI volumes for automatic pancreas segmentation," *Computerized Medical Imaging and Graphics*, vol. 75, pp. 1-13, 2019, doi: 10.1016/j.compmedimag.2019.04.004.
- [31] X. Chen *et al.*, "An efficient multilevel thresholding image segmentation method based on the slime mould algorithm with bee foraging mechanism: A real case with lupus nephritis images," *Computers in Biology and Medicine*, vol. 142, p. 105179, 2022, doi: 10.1016/j.compbiomed.2021.105179.
- [32] G. Li, D. Jiang, Y. Zhou, G. Jiang, J. Kong, and G. Manogaran, "Human lesion detection method based on image information and brain signal," *IEEE Access*, vol. 7, pp. 11533-11542, 2019, doi: 10.1109/ACCESS.2019.2891749.
- [33] S. A. AlDera and M. T. B. Othman, "A model for classification and diagnosis of skin disease using machine learning and image processing techniques," *International Journal of Advanced Computer Science and Applications*, vol. 13, no. 5, pp. 252-259, 2022, doi: 10.14569/ijacsa.2022.0130531.
- [34] M. A. Elaziz, S. Bhattacharyya, and S. Lu, "Swarm selection method for multilevel thresholding image segmentation," *Expert Systems with Applications*, vol. 138, p. 112818, 2019, doi: 10.1016/j.eswa.2019.07.035.
- [35] Z. Faisal and N. K. El Abbadi, "Detection and recognition of brain tumor based on DWT, PCA and ANN," *Indonesian Journal of Electrical Engineering and Computer Science (IJECS)*, vol. 18, no. 1, pp. 56-63, 2019, doi: 10.11591/ijeecs.v18.i1.pp56-63.
- [36] C. Zhang, X. Shen, H. Cheng, and Q. Qian, "Brain tumor segmentation based on hybrid clustering and morphological operations," *International Journal of Biomedical Imaging*, vol. 2019, 2019, doi: 10.1155/2019/7305832.
- [37] R. Kalyani, P. D. Sathya, and V. P. Sakthivel, "Medical image segmentation using exchange market algorithm," *Alexandria Engineering Journal*, vol. 60, no. 6, pp. 5039-5063, 2021, doi: 10.1016/j.aej.2021.04.054.
- [38] A. Abdusalomov, M. Mukhiddinov, O. Djuraev, U. Khamdamov, and T. K. Whangbo, "Automatic salient object extraction based on locally adaptive thresholding to generate tactile graphics," *Applied Sciences*, vol. 10, no. 10, 2020, doi: 10.3390/APP10103350.
- [39] H. Seo, C. Huang, M. Bassenne, R. Xiao, and L. Xing, "Modified U-Net (mU-Net) with incorporation of object-dependent high level features for improved liver and liver-tumor segmentation in CT images," *IEEE Transactions on Medical Imaging*, vol. 39, no. 5, pp. 1316-1325, 2020, doi: 10.1109/TMI.2019.2948320.
- [40] P. Tangwannawit and S. Tangwannawit, "Feature extraction to predict quality of segregating sweet tamarind using image processing," *Indonesian Journal of Electrical Engineering and Computer Science (IJECS)*, vol. 25, no. 1, pp. 339-346, 2022, doi: 10.11591/ijeecs.v25.i1.pp339-346.
- [41] S. M. Rodiah, D. T. Susetianingtias, D. A. Fitrianiingsih, and R. Arianty, "Image processing, pattern recognition retinal biometric identification using convolutional neural network," *Computer Optic*, vol. 45, no. 6, pp. 865-872, 2021, doi: 10.18287/2412-6179-CO-890.
- [42] C. J. J. Sheela and G. Suganthi, "Morphological edge detection and brain tumor segmentation in Magnetic Resonance (MR) images based on region growing and performance evaluation of modified Fuzzy C-Means (FCM) algorithm," *Multimedia Tools Application*, vol. 79, no. 25-26, pp. 17483-17496, 2020, doi: 10.1007/s11042-020-08636-9.
- [43] Sumijan, S. Madenda, J. Harlan, and E. P. Wibowo, "Hybrids Otsu method, feature region and mathematical morphology for calculating volume hemorrhage brain on CT-scan image and 3D reconstruction," *TELKOMNIKA (Telecommunication Comput. Electron. Control)*, vol. 15, no. 1, pp. 283-291, 2017, doi: 10.12928/TELKOMNIKA.v15i1.3146.
- [44] H. A. Saeed, S. Hamad, and A. T. Hussain, "Analysis the digital images by using morphology operators," *Indonesian Journal of Electrical Engineering and Computer Science (IJECS)*, vol. 24, no. 3, pp. 1654-1662, 2021, doi: 10.11591/ijeecs.v24.i3.pp1654-1662.
- [45] H. Huang *et al.*, "Combining adaptive thresholding and region filling for xylene spills detection from ultraviolet images," *2018 Ocean. - MTS/IEEE Kobe Techno-Oceans, Ocean. - Kobe 2018*, pp. 1-6, 2018, doi: 10.1109/OCEANSKOB.2018.8559065.
- [46] O. Tov, Y. Alaluf, Y. Nitzan, O. Patashnik, and D. Cohen-Or, "Designing an encoder for StyleGAN image manipulation," *ACM Transactions on Graphics (TOG)*, vol. 40, no. 4, 2021, doi: 10.1145/3450626.3459838.
- [47] J. Na'am, F. S. Pranata, R. Hidayat, A. M. Adif, and Ellyzartie, "Automated identification model of ground-glass opacity in CT-scan image by COVID-19," *International Journal on Advanced Science, Engineering and Information Technology*, vol. 11, no. 2, pp. 595-602, 2021, doi: 10.18517/ijaseit.11.2.14143.




- [48] G. Yue, W. Han, B. Jiang, T. Zhou, R. Cong, and T. Wang, "Boundary constraint network with cross layer feature integration for polyp segmentation," *IEEE Journal of Biomedical and Health Informatics*, vol. 26, no. 8, pp. 4090-4099, 2022, doi: 10.1109/JBHI.2022.3173948.
- [49] M. S. Nasrabadi and R. Safabakhsh, "3D object recognition with a linear time-varying system of overlay layers," *IET Computer Vision*, vol. 15, no. 5, pp. 380-391, 2021, doi: 10.1049/cvi2.12029.

BIOGRAPHIES OF AUTHORS






Syafri Arlis    was born in Padang, West Sumatra, Indonesia in 1986. Obtained a bachelor's degree in computer science in 2009 and a master's degree in computer science with a concentration in information technology in 2011 at Putra Indonesia University YPTK. Currently active as a computer science lecturer at Putra Indonesia University YPTK. Research work focuses specifically on programming, image processing, and especially medical imaging. He can be contacted at email: syafri_arlis@upiptk.ac.id.



Sarjon Defit    was born in Padang Sibusuk, West Sumatra, Indonesia in 1970. He holds a bachelor's degree in computer science from Putra Indonesia University YPTK and a Master of Science (M.Sc.) and Doctor of Philosophy (Ph.D.) from Universiti Teknologi Malaysia. Currently, he is active as a lecturer in the information technology doctoral program and professor and Chancellor at YPTK Universitas Putra Indonesia. He can be contacted at email: sarjon_defit@upiptk.ac.id.



Sumijan    a lecturer at the Faculty of Computer Science in the Information Technology Program. Born in Nganjuk, East Java, Indonesia in 1966. Obtained a bachelor's degree at Putra Indonesia University YPTK. Then earned an M.Sc. from Universiti Teknologi Malaysia and a Doctor of Information Technology from Gunadarma University in 2015. His work focuses on image processing. He can be contacted at email: sumijan@upiptk.ac.id.